

NANO EXPRESS

Open Access



Optoelectronic Properties of MAPbI₃ Perovskite/Titanium Dioxide Heterostructures on Porous Silicon Substrates for Cyan Sensor Applications

Lung-Chien Chen* and Chiao-Yu Weng

Abstract

This work elucidates the optoelectronic properties of graphene/methylammonium lead iodide (MAPbI₃)/titanium dioxide (TiO₂)/porous Si heterostructure diodes. The porous silicon substrates can accommodate more MAPbI₃/TiO₂ than the polished silicon substrate such that the MAPbI₃/TiO₂/porous Si substrate heterostructures have better optoelectronic properties. Photocurrents from 300 to 900 nm were measured. The photocurrent is high in two ranges of wavelength, which are 300–460 nm and 520–800 nm. The photocurrent plateau covers all visible light (360 to 780 nm) except for cyan between 460 and 520 nm. Therefore, the graphene/MAPbI₃/TiO₂/porous Si heterostructure can be utilized as cyan sensors.

Keywords: Perovskite; TiO₂; Porous silicon; Cyan sensors

Background

Methylammonium lead iodide (CH₃NH₃PbI₃ or MAPbI₃) with the perovskite structure has potential optoelectronic applications, such as solar cells and light-emitting diodes, because of its direct band gap of 1.6 eV, low cost, and ease of production; it has therefore attracted substantial interest [1–5]. MAPbI₃ perovskite-based solar cells with a power conversion efficiency of over 20 % have been successfully developed [6]. Such solar cells are promising because of their low cost, simplicity of fabrication, and absorption in the solar spectrum as well as balanced charge transport characteristics with long diffusion lengths [7, 8]. Light-emitting diodes that are based on halide perovskite have also been fabricated [9]. The green light-emitting device with the ITO/PEDOT:PSS/MAPbBr₃/F8/Ca/Ag structure has a luminance of 364 cd/m² at a current density of 123 mA/cm² and external and internal quantum efficiencies of 0.1 and 0.4 %, respectively.

Last year, several works on perovskite-based photodetectors have been published [10, 11]. The absorption range of the MAPbI₃ is very broad. The typical range is from 300 to 800 nm. However, excellent absorption of light cannot transform the absorbed energy into a

photocurrent. Therefore, in this study, we developed the graphene/CH₃NH₃PbI₃ (MAPbI₃) perovskite/titanium dioxide (TiO₂)/porous silicon substrate heterostructure diodes and studied their structure and optoelectronic properties.

Methods

Single crystalline (100) p-type boron-doped Si substrates with a resistivity of 10 Ω cm were used in this study. Prior to processing, the wafers were cut into 1 × 1 cm² and cleaned by ultrasonication in acetone, ethanol, and deionized water, consecutively. The silicon wafers then were immersed in dilute hydrogen fluoride (HF) solution to remove the native oxide layers, yielding a hydrogen-terminated surface. Next, the porous silicon structure was fabricated by metal-assisted chemical etching (MACE) in the freshly prepared dilute solution that contained both HF (48 %) and AgNO₃ (0.02 mol/l) (1:1) with different etching times at room temperature. When the Si wafer was dipped into the etching solution, a silver nano-cluster layer was formed on its surface. The wafer was then put in a dilute HNO₃ solution (50 wt%) to remove the Ag layer.

The TiO₂ layer was coated onto the silicon substrate at a speed of 2000 rpm for 10 s and then annealed at 550 °C for 30 min. Subsequently, MAPbI₃ perovskite

* Correspondence: ocean@ntut.edu.tw
Department of Electro-optical Engineering, National Taipei University of Technology, 1, sec.3, Chung-Hsiao E. Rd., Taipei 106, Taiwan

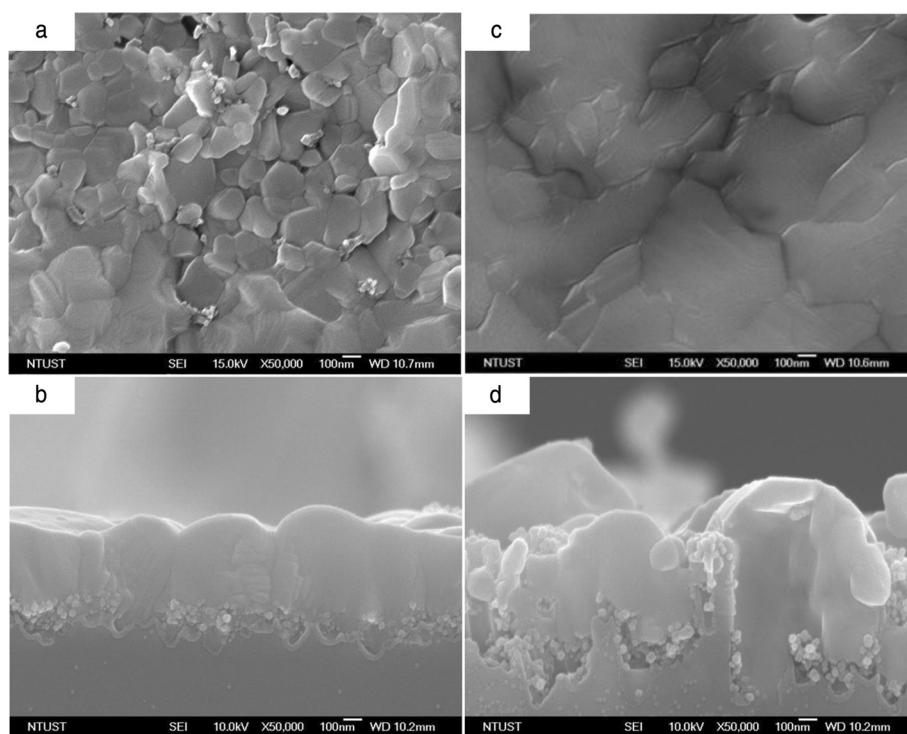


Fig. 1 Schematic top view (a, c) and cross section (b, d) of MAPbI₃/TiO₂ on porous Si heterostructure

precursor solution was coated onto the surface of the TiO₂/silicon substrates using a spinner at a speed of 5000 rpm for 20 s. In this study, the perovskite layer was deposited by the solvent-engineering technology of 1.2 M PbI₂ and 1.2 M methylammonium iodide (MAI) in a cosolvent of dimethyl sulfoxide (DMSO) and γ -butyrolactone (GBL) (vol. ratio = 1:1) in a glove box filled with highly pure nitrogen. Then, the substrate was annealed at 100 °C for 10 min. The graphene layer was spin-coated using DMF-based graphene suspension (0.3 mg/ml) at 2000 rpm for 20 s. Finally, an indium contact ($\sim 2 \mu\text{m}$) was evaporated onto the top of the graphene electron-spreading layer to complete the whole diode structure. The morphology and cross section of the resulting structures were examined using field emission scanning electron microscopy (FESEM). Photoluminescence (PL) was measured at room temperature. The excitation source for PL was a 405-nm diode laser. The electronic characteristics were measured using a Keithley 2420 programmable source meter.

Results and Discussion

Figure 1 displays the top and cross-sectional FESEM images of the MAPbI₃ perovskite/TiO₂ on the porous Si substrates after etching for various times. Figure 1a, b presents the top and cross-sectional FESEM images of the MAPbI₃ perovskite/TiO₂ on the porous Si substrates that had been etched for 5 min. Figure 1c, d presents the

top and cross-sectional FESEM images of the MAPbI₃ perovskite/TiO₂ on the porous Si substrates after etching for 10 min. The MAPbI₃ perovskite was coated on the TiO₂ layer, and the interface between the MAPbI₃ perovskite and TiO₂ layer formed the heterojunction. As presented in Fig. 1b, d, the MAPbI₃ perovskite/TiO₂ heterojunction penetrated into the porous silicon substrate. The thickness of the MAPbI₃ perovskite films on the 5- and 10-min etched porous silicon substrates was around 500 nm.

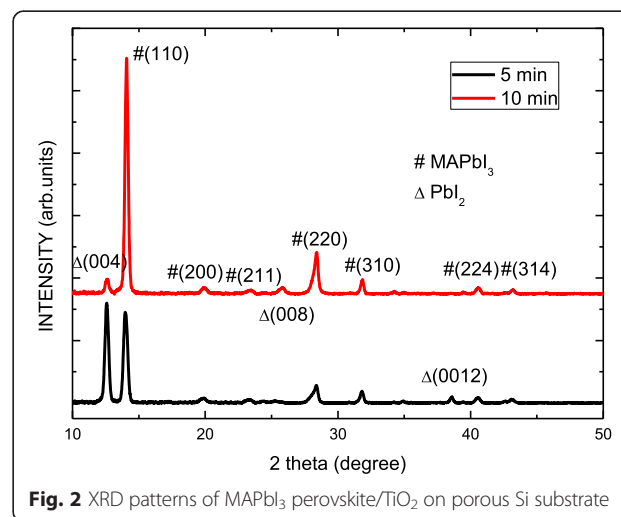


Fig. 2 XRD patterns of MAPbI₃ perovskite/TiO₂ on porous Si substrate

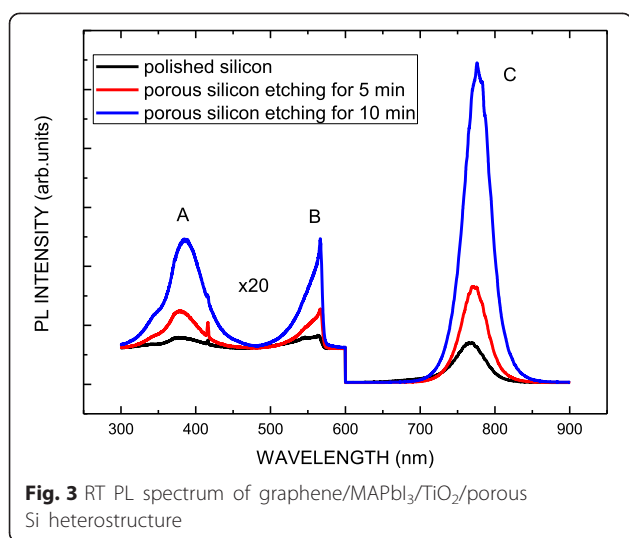
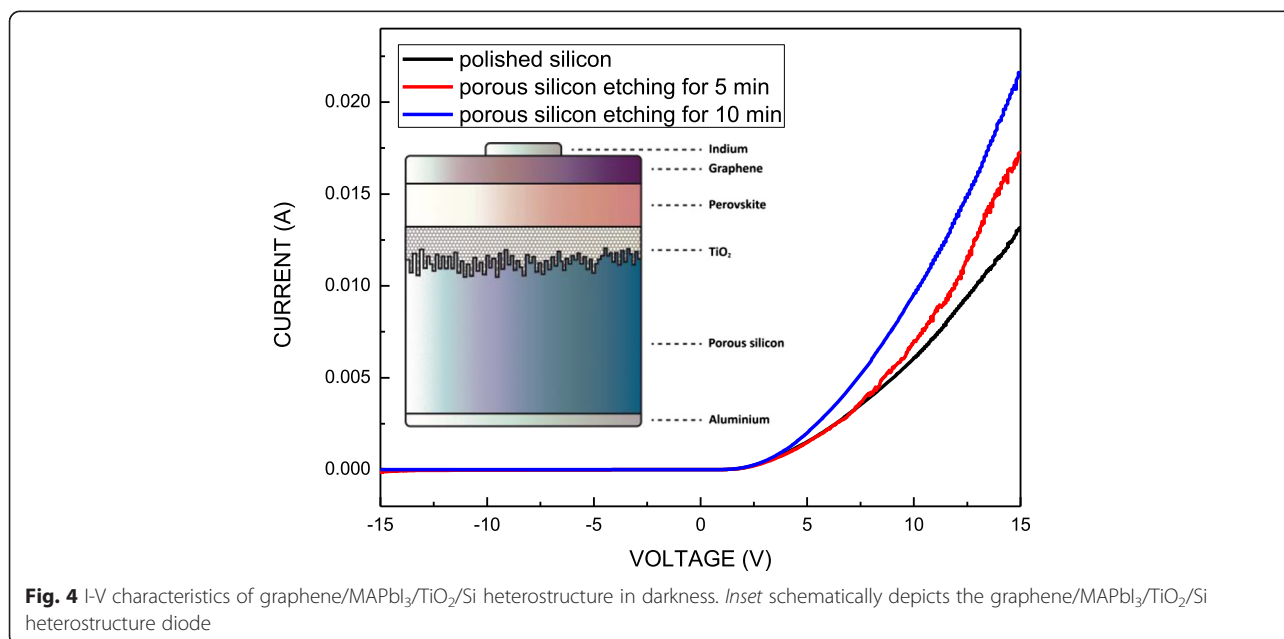


Figure 2 shows the XRD patterns of the MAPbI₃ perovskite/TiO₂ on the porous Si substrate following etching for 5 and 10 min. The spectra include seven main peaks at 14.08°, 19.9°, 23.3°, 28.42°, 31.85°, 40.28°, and 43.21°, which correspond to the (110), (200), (211), (220), (310), (224), and (314) for the CH₃NH₃PbI₃ perovskite, respectively. However, the PbI₂ (004), (008), and (0012) peaks located at 12.58°, 25.81°, and 38.58°, respectively, can be observed in both samples. The co-existence of the two CH₃NH₃PbI₃ and PbI₂ phases can be observed in the MAPbI₃ perovskite layers. This is due to the post annealing process leading to thermal decomposition of MAI and the formation of the PbI₂ phase. Previous reports using transient photoluminescence exhibit the presence of the PbI₂ in MAPbI₃ active light

harvesting layers that can enhance the carrier transportation to the electrode [12–14]. On the other hand, to further elucidate detailed structural information, the grain size G was calculated according to Scherrer's equation [15]. The G grain sizes of the samples that were etched for 5 and 10 min are 22.2 and 29.5 nm, respectively. The quality of MAPbI₃ on the porous silicon substrate with etching for 10 min is higher than that of the sample following etching for 5 min. The strongest signal from the samples with etching for 5 min is that of the (110) plane. However, the most intense signal of the samples that were etched for 10 min is that of the (101) plane. The morphology of the Si substrate influences the formation of the crystalline MAPbI₃.

Figure 3 shows the room-temperature photoluminescence (RT PL) spectrum of the MAPbI₃/TiO₂/porous Si heterostructure. From all samples, the dominant peak at 1.6 eV (776 nm), labeled C, corresponds to the optical band gap of the MAPbI₃ films, which have a direct band gap that can be attributed to the recombination of the near band-to-band (B-B) [1, 16]. Other than peak C, two weak peaks, A and B, are observed. The A peak at 382 nm corresponds to the recombination of the B-B of TiO₂ [17]. Peak B at 566 nm is associated with the emission from defects in TiO₂ [17–19]. The PL intensity increases with the etching time of the silicon substrate. That may be attributed to the amount of the TiO₂ and MAPbI₃ penetrated into the porous silicon substrates to fill in the porous increases due to the dimension increase of the porous when etching time increases.

Figure 4 plots the I-V characteristics of the graphene/MAPbI₃/TiO₂/porous Si heterostructure diode in darkness. The turn-on voltage of the graphene/MAPbI₃/TiO₂/porous



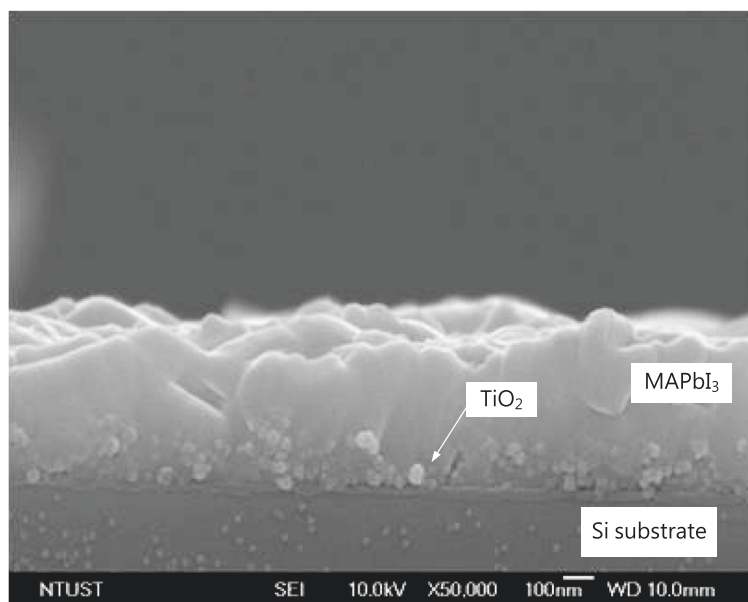


Fig. 5 Cross-sectional FESEM image of the MAPbI₃/TiO₂ on polished silicon substrate

Si heterostructure diode is approximately 2.5 V, and its breakdown voltage is over 15 V. The inset schematically depicts the graphene/MAPbI₃/TiO₂/porous Si heterostructure diode. The graphene/MAPbI₃/TiO₂/porous Si that was etched for 10 min exhibited the lowest series resistance, because it had the highest effective contact area of porous silicon and accommodated the largest MAPbI₃/TiO₂ bulk junction, relative to the polished silicon substrate, as shown in Figs. 1b, d and 5. As mentioned above, the purity and grain size of MAPbI₃ on the porous silicon substrate with etching for 10 min is higher than that of the sample with etching for 5 min. It is believed that the TiO₂ nanoparticle deposited on the substrate etched for 10 min can provide more surface area and good contact, leading to less MAI loss and better crystal quality. The morphology of the Si substrate influences the formation of the crystalline MAPbI₃ and optoelectronic characteristics of MAPbI₃-based devices.

Figure 6 plots the photocurrent as a function of the wavelength of incident light for a graphene/MAPbI₃/TiO₂/porous Si heterostructure at a reverse bias of 5 V. The photocurrent is high in two ranges of wavelength from 300 to 450 nm and from 520 to 780 nm. The former corresponds to TiO₂ and the latter corresponds to the MAPbI₃. Two photocurrents tail off at wavelengths of 460 and 780 nm. As compared to the pure TiO₂ with an absorption edge of 400 nm, the tailing off at 460 nm suggests the presence of traps in the band gap of the TiO₂ that are generated by the presence of impurities from MAPbI₃ [20]. The tailing off at 770 nm suggests the band gap 1.6 eV of the MAPbI₃. The

photocurrent plateau covers all visible wavelengths (360 to 780 nm) except for those of cyan from 460 to 520 nm. Therefore, the graphene/MAPbI₃/TiO₂/porous Si heterostructure can be used in a cyan sensor.

Conclusions

The optoelectronic characteristics of graphene/MAPbI₃/TiO₂/Si heterostructure diodes were investigated. As the etching time of the silicon substrate increased, the PL intensity increased, because more TiO₂ and MAPbI₃ penetrated into the porous silicon substrates, because they accommodated more MAPbI₃/TiO₂. The MAPbI₃/TiO₂ on the porous silicon substrate increased the

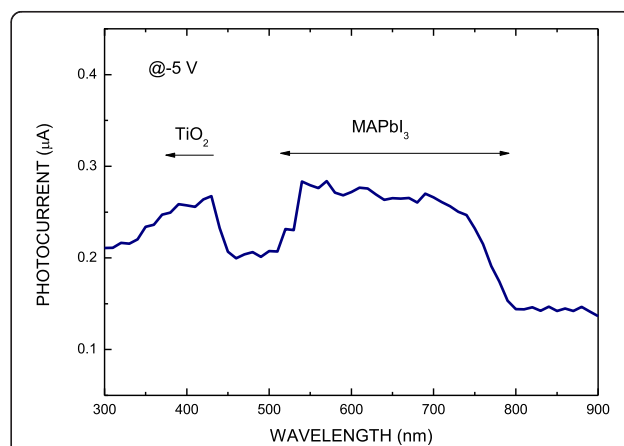


Fig. 6 Photocurrent as a function of wavelength of incident light for a graphene/MAPbI₃/TiO₂/porous Si heterostructure at a bias of 5 V

effective contact area of the heterostructure and reduced its series resistance. The photocurrent plateau covered all visible wavelengths (360 to 780 nm), except for those of cyan from 460 to 520 nm. Therefore, as shown in Fig. 6, the graphene/MAPbI₃/TiO₂/porous Si heterostructure can not only be utilized in a cyan sensor but also for near-IR light (780–900 nm or more) applications.

Competing interests

The authors declare that they have no competing interests.

Authors' contributions

LCC wrote the paper, designed the experiments, and analyzed the data. CYW prepared the samples and did all the measurements. Both authors read and approved the final manuscript.

Acknowledgements

Financial support of this paper was provided by the Ministry of Science and Technology of the Republic of China under Contract No. MOST 103-2221-E-027-029-MY2.

Received: 22 September 2015 Accepted: 9 October 2015

Published online: 16 October 2015

References

- Agiorgousis ML, Sun YY, Zeng H, Zhang SJ (2014) Strong covalency-induced recombination centers in perovskite solar cell material CH₃NH₃PbI₃. *J Am Chem Soc* 136:14570–14575.
- Momblona C, Malinkiewicz O, Roldán-Carmona C, Soriano A, Gil-Escrig L, Bandiello E, Scheepers M, Edri E, Bolink HJ (2014) High performance perovskite solar cells by hybrid chemical vapor deposition. *APL Mater* 2:081504.
- Carnie MJ, Charbonneau C, Davies ML, Troughton J, Watson TM, Wojciechowski K, Snaith H, Worsley DA (2013) A one-step low temperature processing route for organolead halide perovskite solar cells. *Chem Commun* 49:7893–7895.
- Cohen BE, Gamliel S, Etgar L (2014) Parameters influencing the deposition of methylammonium lead halide iodide in hole conductor free perovskite-based solar cells. *APL Mater* 2:081502.
- Lee M, Jo, Y, Kim DS, Jeong HY, Jun Y (2015) Efficient, durable and flexible perovskite photovoltaic devices with Ag-embedded ITO as the top electrode on a metal substrate. *J Mater Chem A* doi:10.1039/c5ta03240g.
- Yang WS, Noh JH, Jeon NJ, Kim YC, Ryu S, Seo J, Seok SI (2015) High-performance photovoltaic perovskite layers fabricated through intramolecular exchange. *Science* 348:1234–1237.
- Jung HS, Park NG (2015) Perovskite solar cells: from materials to devices. *Small* 11:10–25.
- Chen LC, Chen YH (2015) TiO₂ dye-sensitized solar cells with perovskite sensitized layer. *Sci Adv Mater* 7:1636–1639.
- Tan ZK, Moghaddam RS, Lai ML, Docampo P, Higler R, Deschler F, Price M, Sadhanala A, Pazos LM, Credgington D, Hanusch F, Bein T, Snaith HJ, Friend RH (2014) Bright light-emitting diodes based on organometal halide perovskite. *Nature Nanotech* 9:687–692.
- Lee Y, Kwon J, Hwang E, Ra CH, Yoo WJ, Ahn JH, Park JH, Cho JH (2015) High-performance perovskite-graphene hybrid photodetectors. *Adv Mater* 27:41–46.
- Horváth E, Spina M, Szekrényes Z, Kamarás K, Gaal R, Gachet D, László F (2014) Nanowires of methylammonium lead iodide (CH₃NH₃PbI₃) prepared by low temperature solution-mediated crystallization. *Nano Lett* 14:6761–6766.
- Song TB, Chen Q, Zhou H, Luo S, Yang YM, You J, Yang Y (2015) Unraveling film transformations and device performance of planar perovskite solar cells. *Nano Energy* 12:494–500.
- Chen Q, Zhou H, Song TB, Luo S, Hong Z, Duan HS, Dou L, Liu Y, Yang Y (2014) Controllable self-induced passivation of hybrid lead iodide perovskites toward high performance solar cells. *Nano Lett* 14(7):4158–4163.
- Liu M, Johnston MB, Snaith HJ (2013) Efficient planar heterojunction perovskite solar cells by vapour deposition. *Nature* 501:395–398.
- Hsu CH, Chen LC, Zhang X (2014) Effect of the Cu source on optical properties of CuZnO films deposited by ultrasonic spraying. *Materials* 7:1261–1270.
- Im JH, Kim HS, Park NG (2014) Morphology-photovoltaic property correlation in perovskite solar cells: one-step versus two-step deposition of CH₃NH₃PbI₃. *APL Mat* 2:081510.
- Li W, Bai Y, Liu W, Liu C, Yang Z, Feng X, Lu X, Chan KY (2011) Single-crystalline and reactive facets exposed anatase TiO₂ nanofibers with enhanced photocatalytic properties. *J Mater Chem* 21:6718–6724.
- Liu B, Peng L (2013) Facile formation of mixed phase porous TiO₂ nanotubes and enhanced visible-light photocatalytic activity. *J Alloys Compounds* 571:145–152.
- Tang H, Berger H, Schmid PE, Lévy F (1993) Photoluminescence in TiO₂ anatase single crystals. *Solid State Commun* 87:847–850.
- Li X, Li X, Luo Q, Wang D, An J, Li X (2015) Effect of conditions for preparation of cyclized polyacrylonitrile sensitized TiO₂ nanoparticles on visible-light photocatalysis and photo absorbance property. *Environ Prog Sustain Energy* 34:32–38.

Submit your manuscript to a SpringerOpen® journal and benefit from:

- Convenient online submission
- Rigorous peer review
- Immediate publication on acceptance
- Open access: articles freely available online
- High visibility within the field
- Retaining the copyright to your article

Submit your next manuscript at ► springeropen.com